PIC simulations of overstretched ion-scale current sheets in the magnetotail

Harry Arnold[1] and Mikhail I. Sitnov[2]

[1]Johns Hopkins University Applied Physics Labs
[2]JHU/APL

May 25, 2023

Abstract

Onset of reconnection in the tail requires the current sheet thickness to be of the order of the ion thermal gyroradius or smaller. However, existing isotropic plasma models cannot explain the formation of such thin sheets at distances where the X-lines are typically observed. Here we reproduce such thin and long sheets in particle-in-cell simulations using a new model of their equilibria with weakly anisotropic ion species assuming quasi-adiabatic ion dynamics, which substantially modifies the current density. It is found that anisotropy/agyrotropy contributions to the force balance in such equilibria are comparable to the pressure gradient in spite of weak ion anisotropy. New equilibria whose current distributions are substantially overstretched compared to the magnetic field lines are found to be stable in spite of the fact that they are substantially longer than isotropic sheets with similar thickness.

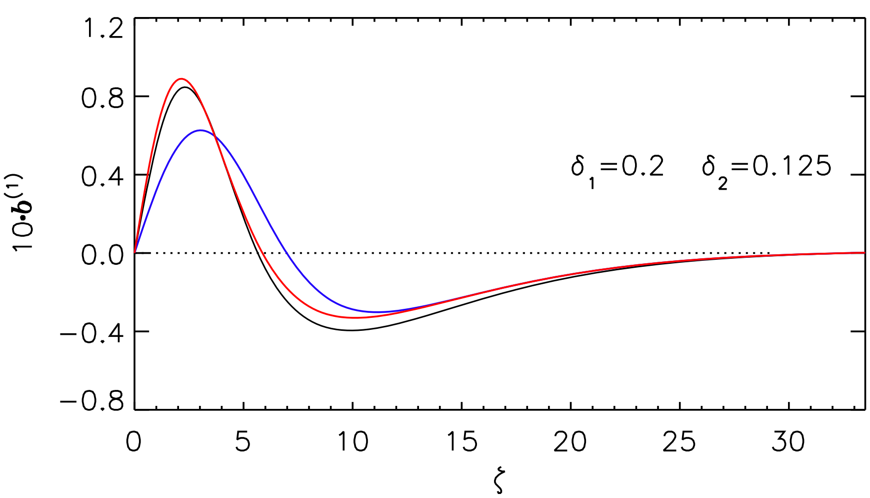

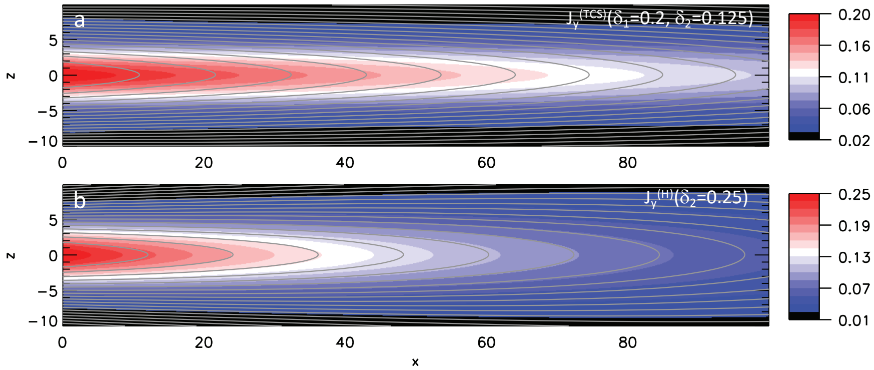
a
$J_y^{(TCS)}(\delta_1=0.2, \delta_2=0.125)$
b
$J_y^{(H)}(\delta_2=0.25)$
z
x
0.20
0.16
0.11
0.06
0.02
0.25
0.19
0.13
0.07
0.01

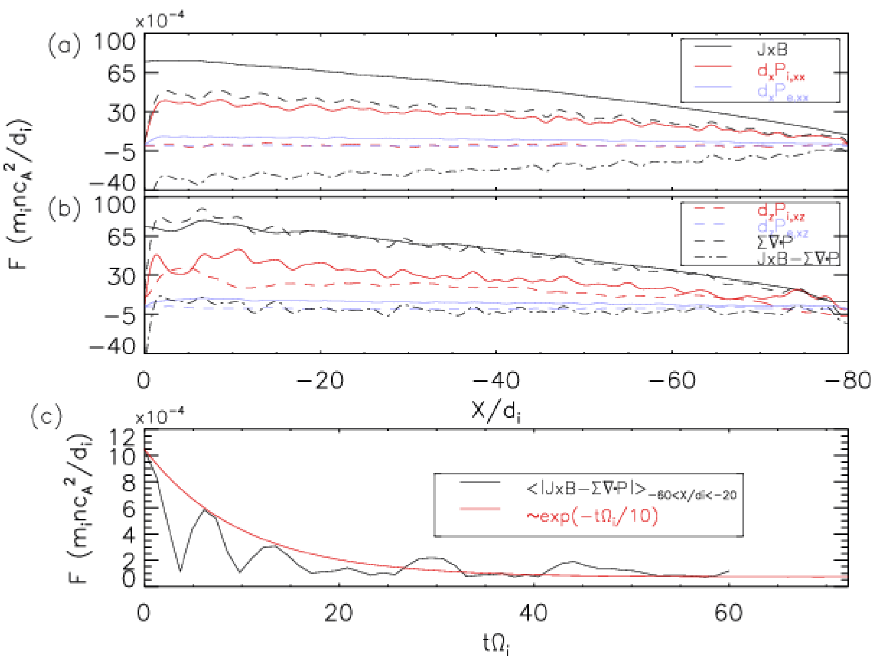
(a)
(b)
(c)
$\times10^{-4}$
JxB
$d_xP_{i,xx}$
$d_xP_{e,xx}$
$d_zP_{i,xz}$
$d_zP_{e,xz}$
$\Sigma\nabla\cdot P$
$JxB-\Sigma\nabla\cdot P$
$F\ (m_inc_A^2/d_i)$
X/d_i
$<|JxB-\Sigma\nabla\cdot P|>_{-60<X/di<-20}$
$\sim\exp(-t\Omega_i/10)$
$t\Omega_i$

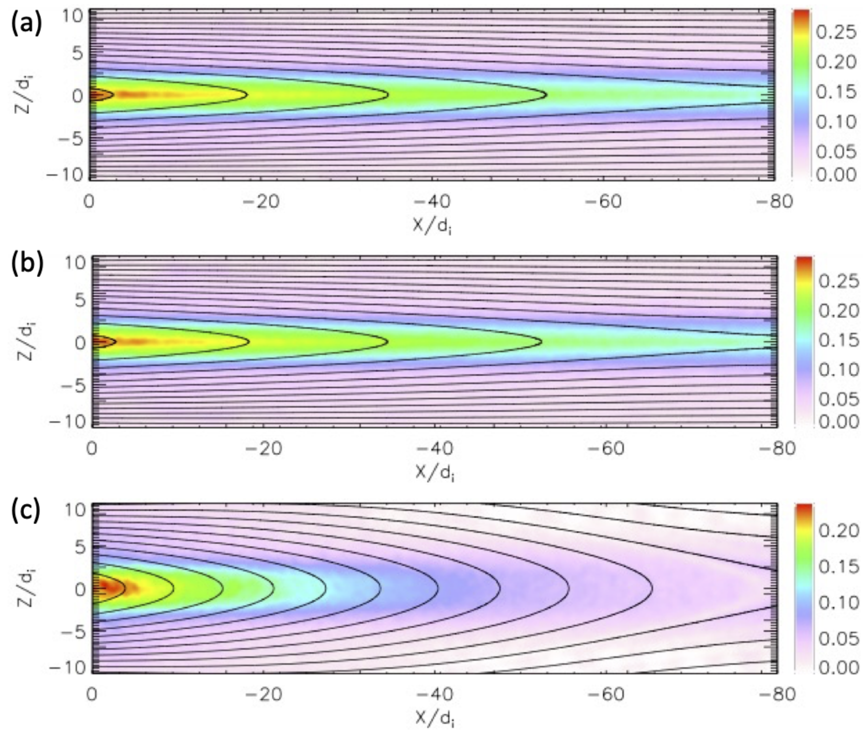
(a)
(b)
(c)
Z/d_i
X/d_i

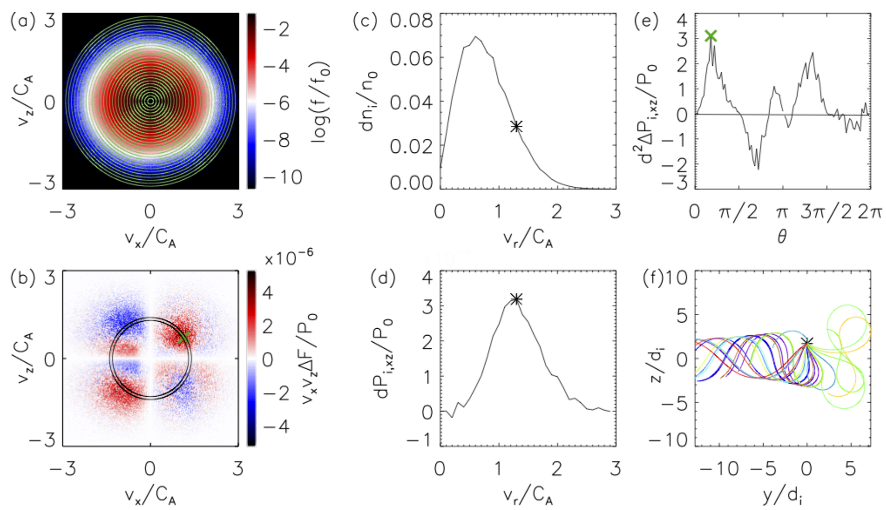
(a)
(b)
(c)
(d)
(e)
(f)
log(f/f_0)
v_z/C_A
v_x/C_A
×10^−6
v_x v_z ΔF/P_0
dn_i/n_0
v_r/C_A
dP_i,xz/P_0
d^2ΔP_i,xz/P_0
θ
z/d_i
y/d_i

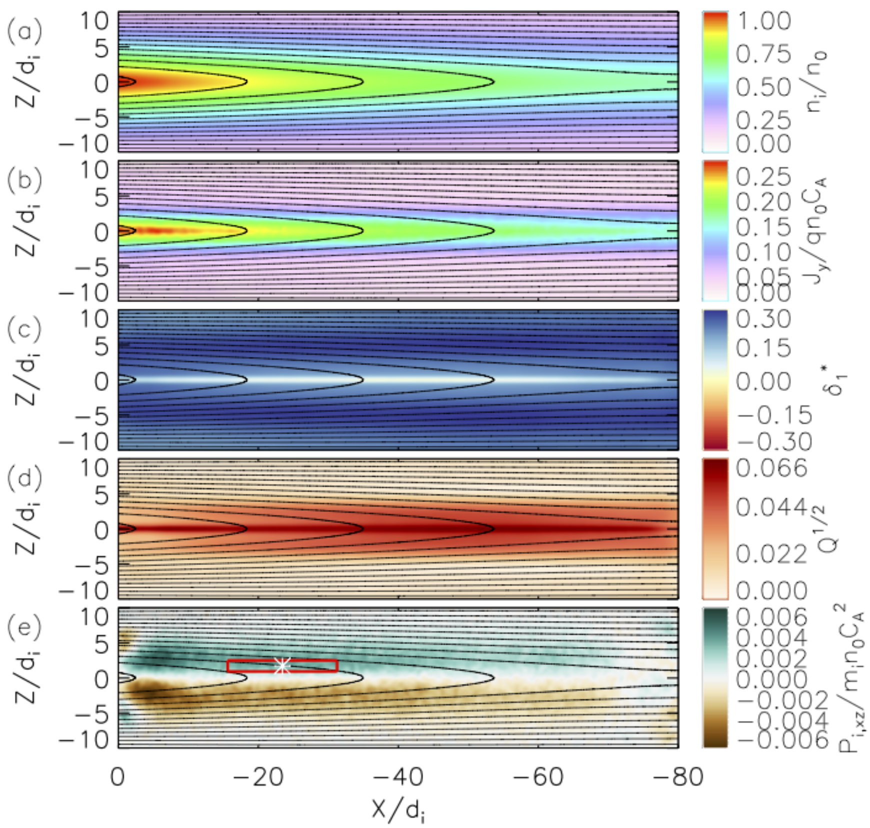

(a)
(b)
(c)
(d)
(e)
Z/d_i
X/d_i
n_i/n_0
J_y/qn_0C_A
δ_1*
Q^{1/2}
P_{i,xz}/m_in_0C_A^2

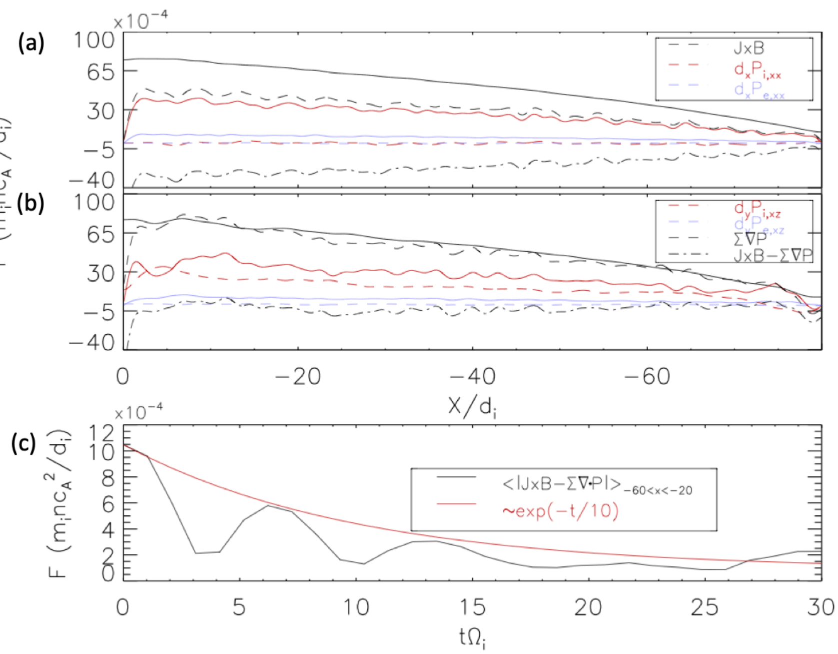

(a)
(b)
(c)
x10^-4
JxB
d_xP_{i,xx}
d_xP_{e,xx}
d_zP_{i,xz}
d_zP_{e,xz}
Σ∇P
JxB−Σ∇P
F (m_inc_A^2/d_i)
X/d_i
<|JxB−Σ∇P|>_{-60<x<-20}
~exp(−t/10)
tΩ_i

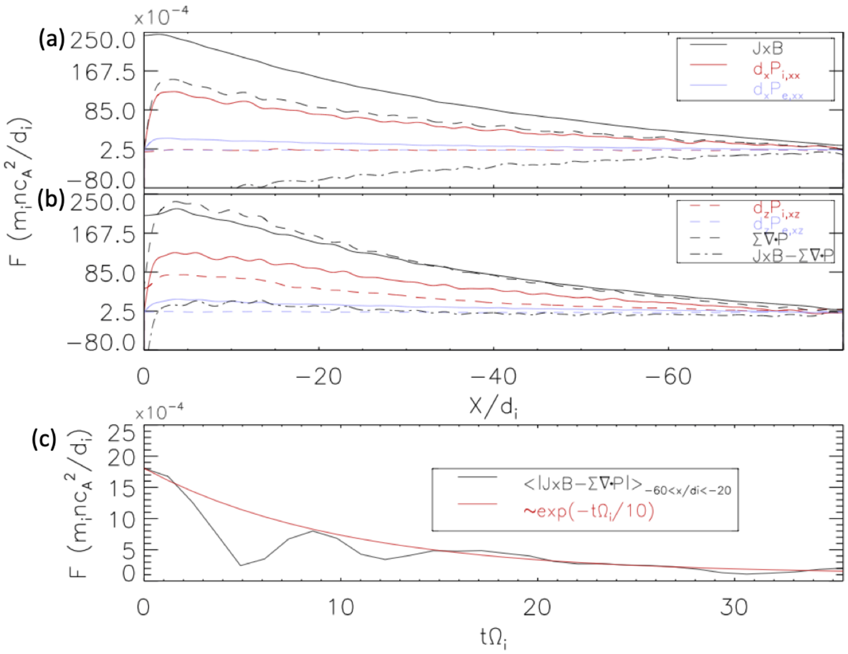
(a)
(b)
(c)
×10⁻⁴
JxB
$d_xP_{i,xx}$
$d_xP_{e,xx}$
$d_zP_{i,xz}$
$d_zP_{e,xz}$
$\Sigma\nabla\cdot P$
$JxB-\Sigma\nabla\cdot P$
$F\ (m_inc_A^2/d_i)$
X/d_i
$<|JxB-\Sigma\nabla\cdot P|>_{-60<x/di<-20}$
$\sim\exp(-t\Omega_i/10)$
$t\Omega_i$

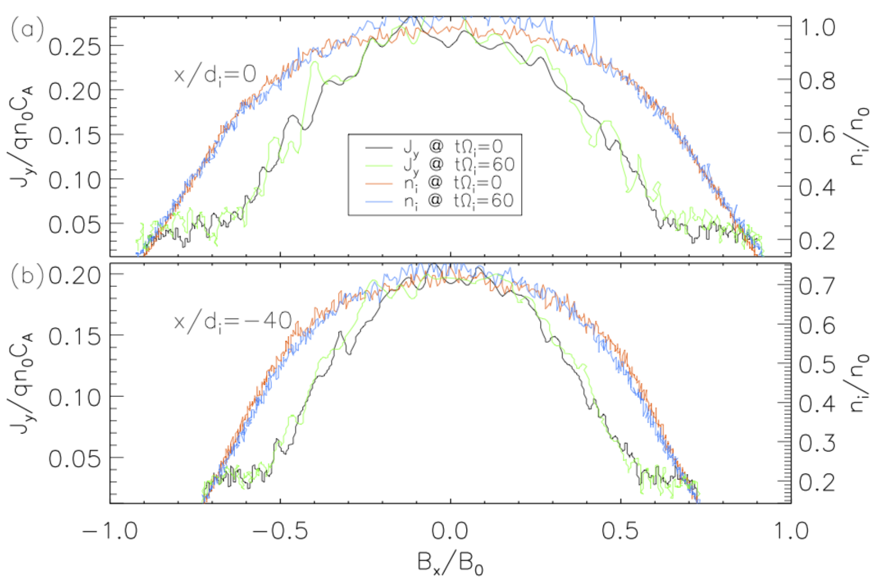
(a)
(b)
$x/d_i=0$
$x/d_i=-40$
J_y @ $t\Omega_i=0$
J_y @ $t\Omega_i=60$
n_i @ $t\Omega_i=0$
n_i @ $t\Omega_i=60$
J_y/qn_0C_A
n_i/n_0
B_x/B_0

PIC simulations of overstretched ion-scale current sheets in the magnetotail

H. Arnold[1], **M. I. Sitnov**[1]

[1]The Johns Hopkins University Applied Physics Laboratory, Laurel, Maryland, USA.

Key Points:

- Two-dimensional ion-scale current sheets stretched way beyond the isotropic limit are reproduced in particle-in-cell simulations
- Weak ion anisotropy and agyrotropy substantially modify the current density and the isotropic force balance
- Ion-scale current sheets are stable in spite of the fact that they are longer compared to isotropic sheets with similar thickness

Corresponding author: M. I. Sitnov, `Mikhail.Sitnov@jhuapl.edu`

Abstract

Onset of reconnection in the tail requires the current sheet thickness to be of the order of the ion thermal gyroradius or smaller. However, existing isotropic plasma models cannot explain the formation of such thin sheets at distances where the X-lines are typically observed. Here we reproduce such thin and long sheets in particle-in-cell simulations using a new model of their equilibria with weakly anisotropic ion species assuming quasi-adiabatic ion dynamics, which substantially modifies the current density. It is found that anisotropy/agyrotropy contributions to the force balance in such equilibria are comparable to the pressure gradient in spite of weak ion anisotropy. New equilibria whose current distributions are substantially overstretched compared to the magnetic field lines are found to be stable in spite of the fact that they are substantially longer than isotropic sheets with similar thickness.

Plain Language Summary

Ion scale current sheets forming sufficiently far from the Earth are necessary to explain its magnetic field reconfiguration on the night side. However, these cannot be formed in isotropic plasmas because then they would inflate too rapidly. We present kinetic simulations of current sheets that inflate much slower due to slight field-aligned anisotropy of the ion species. Their formation is provided by a special population of suprathermal ions with figure-of-eight orbits. We find that the resulting current sheets are stable over a long time scale and have a thickness comparable to the size of these orbits.

1 Introduction

The mechanism of slow energy accumulation and its rapid release in the magnetotail during substorms remains a fundamental unsolved problem of magnetospheric physics (McPherron, 2016; M. Sitnov et al., 2019). During the substorm growth phase, magnetic flux is transported from the day side to the night side of Earth's magnetosphere to stretch and thin the tail current sheet (CS) making it susceptible to spontaneous magnetic reconnection (Coppi et al., 1966; Schindler, 1974). Conventional CS equilibria with gyrotropic plasmas cannot explain the observed aspect ratio of the CS whose thickness is comparable to the ion gyroradius, ρ_{0i}, based on the field, B_0, outside the CS (Runov et al., 2005) while its length may be two orders of magnitude larger (Artemyev et al., 2015; M. I. Sitnov et al., 2019) As a result, kinetic simulations of the reconnection onset, independent of the specific mechanism, ion tearing (M. I. Sitnov et al., 2013; Bessho & Bhattacharjee, 2014; Pritchett, 2015) or electron tearing (Hesse & Schindler, 2001; Liu et al., 2014), show the X-line formation within a few Earth radii ($\lesssim 20\rho_{0i}$) from the left boundary corresponding to the near-Earth end of the tail, where it is observed only in very rare cases (Angelopoulos et al., 2020). Meanwhile, thin ion-scale current sheets are routinely observed farther in the tail ($\gtrsim 20R_E \sim 200\rho_{0i}$, where R_E is the Earth's radius) (Runov et al., 2005; Artemyev et al., 2015) where the X-lines usually form (Nagai et al., 2005, 2015; Eastwood et al., 2010; Stephens et al., 2023).

Typically, theoretical descriptions of the magnetotail CS, including initialization of kinetic simulations, are performed using 2-D generalizations of the 1-D Harris model (Harris, 1962), which can be applied when the normal to the CS magnetic field component $B_z = 0$. The Harris model is based on the plasma distribution functions dependent on invariants of particle motion, the total energy $W_\alpha = m_\alpha v^2/2+q_\alpha\phi$ and the y-component of the canonical momentum $P_{y\alpha} = m_\alpha v_y + (q_\alpha/c)A_y$, where $\alpha = i, e$ is the species index for ions and electrons, ϕ is the electrostatic potential and $\mathbf{A} = (0, A_y(z), 0)$ is the vector potential. The use of these invariants allows one to automatically obey the stationary Vlasov equation. 2D generalizations of the Harris model with applications to the magnetotail are obtained in the stretched magnetic field approximation $0 < B_z/B_0 \ll 1$ (Schindler, 1972; Lembege & Pellat, 1982).

The dependence of distributions on the total energy and canonical momentum imposes the following relation between the pressure gradient and the Lorentz force: $\partial P_{xx}/\partial x = (\partial p/\partial A_y)(\partial A_y/\partial x) = j_y B_z$. This relation is valid both for isotropic models where W_α and $P_{y\alpha}$ enter the distribution in a linear combination (Lembege & Pellat, 1982) and for more complex anisotropic Harris-type models (Schindler & Birn, 2002; Birn et al., 2004). It implies that the Lorentz force along the tail in these CS is balanced by the plasma pressure. In view of the force balance across the CS, it also implies that the CS length L_x is related to its thickness L_z as $L_x/L_z \sim B_0/B_z$. Since typical values of B_0/B_z do not exceed ~ 20 (Figure 3 in (Artemyev, Angelopoulos, & Runov, 2016), Figure 15 in (M. I. Sitnov et al., 2019)), it also means that the length of the ion-scale thin current sheets (TCS) cannot exceed $\sim 20\rho_{0i}$. Since for typical plasma parameters $\rho_{0i} \sim 0.1R_E$ (e.g., Runov et al., 2005), the radial extension of such TCS cannot exceed $2R_E$. As a result, it becomes impossible to explain the formation of TCS sufficiently far from the dipolar field region. Note that in all models without X-lines ($B_z > 0$) the TCS thickness L_z increases with the distance from Earth (e.g., Schindler, 1972).

According to Rich et al. (1972), the problem of insufficient TCS stretching cannot be solved due to the inertial terms in the momentum equation and hence it cannot be solved due to dynamical effects in MHD simulations that usually employ isotropic plasma models (e.g. Merkin et al., 2019). It can be solved however due to plasma anisotropy through additional (off-diagonal) pressure terms in the force balance equation (Rich et al., 1972)

$$\frac{\partial(P_{exx} + P_{ixx})}{\partial x} + \frac{\partial P_{exz}}{\partial z} + \frac{\partial P_{ixz}}{\partial z} = j_y B_z \tag{1}$$

In the gyrotropic approximation these off-diagonal terms on the left hand side of (1) can be reduced to $P_{xz} = (P_{||} - P_\perp)B_x B_z/B^2$, where $p_{||}$ and $p_\perp$ are the plasma pressure components parallel and perpendicular to the plasma sheet. Indeed, a number of models employing different equations of state for electron species have been proposed (L. M. Zelenyi et al., 2004; Egedal et al., 2013; Artemyev, Vasko, et al., 2016). Moreover, the importance of the electron anisotropy for reconnection outflow regions was explicitly demonstrated in particle-in-cell (PIC) simulations (Le et al., 2019, and refs. therein). Meanwhile, Egedal et al. (2013) and Artemyev, Vasko, et al. (2016) showed that new TCS equilibria become possible due to an additional integral of motion in the electron distribution, the magnetic moment $\mu = m_e v_\perp^2/(2B)$.

However, closer examination shows that the electron anisotropy as well as the gyrotropic plasma approximation are insufficient to explain the observed global and local structure of the magnetotail TCS. First, on average, the electron anisotropy is rather small. According to (Artemyev et al., 2012, Figure 4), the electron temperature anisotropy is about 5%. Taking into account that electrons are substantially colder than ions in the tail plasma sheet with T_i/T_e varying from $\sim$ 2 to 12 (Artemyev, Baumjohann, et al., 2011; Wang et al., 2012), their anisotropy values are equivalent to $\sim 1\%$ ion anisotropy. Unsurprisingly, the electron temperature anisotropy force (the second term in (1)) can balance only 10–15% of the observed tension force $j_y B_z$ (Artemyev, Angelopoulos, & Runov, 2016).

Meanwhile, the observed values of the ion anisotropy are an order of manuitude larger: Geotail observations (Kaufmann et al., 2000) suggest that $T_{i||}/T_{i\perp} \approx 1.2$ in the range of the plasma beta $0.1 < \beta < 3$ in the spatial region $-31R_E < x < -19R_E$ $|y| < 6R_E$. THEMIS observations (Artemyev et al., 2019) suggest comparable values of anisotropy in similar regions for quiet tail conditions. Finally, combined data from Cluster and THEMIS for CS thinning periods (Yushkov et al., 2021, Figure 10) show that for many (15 out of 20 events, with most negative cases being found at the near-Earth edge of the tail CS) the field-aligned ion anisotropy reaches $\sim 10\%$ at the end of the thinning period. Yet, even the ion anisotropy is rather weak ($T_{i||}/T_{i\perp} - 1 \ll 1$), and it is not clear if it can substantially modify the tail force balance (1) and the TCS aspect ratio L_x/L_z compared to its isotropic estimate B_0/B_z.

Second, in the tail TCS with the half-thickness $L_z \sim \rho_{0i}$ and $B_z/B_0 \ll 1$ the thermal ion population is not adiabatic but rather quasi-adiabatic, which is seen from the simplified adiabaticity parameter (Büchner & Zelenyi, 1989) $\kappa = (B_z/B_0)\sqrt{L_z/\rho_{0i}} \ll 1$. In this regime the magnetic moment is not conserved because the ion orbits deviate from their Larmor gyration and instead resemble a figure of eight (the so-called Speiser orbits (Speiser, 1965)). As was shown in (Schindler, 1965; Sonnerup, 1971; Büchner & Zelenyi, 1989) for this regime one can use another quasi-adiabatic invariant of motion

$$I_z^{(i)} = \frac{1}{2\pi}\oint m_i v_z dz \tag{2}$$

Since ions on Speiser orbits are not magnetized by the field B_z they can provide Landau dissipation (Pritchett et al., 1991) critical for the ion tearing instability (Schindler, 1974; M. I. Sitnov & Schindler, 2010; M. I. Sitnov & Swisdak, 2011; M. I. Sitnov et al., 2018). Speiser ion motions should also make plasma agyrotropic. Indeed, recent MMS observations (Motoba et al., 2022) revealed substatial ion agyrotropy quantified by Swisdak's Q-parameter (Swisdak, 2016).

In this Letter we show that even small ion anisotropy, similar to the aforementioned observations, can substantially modify the force balance (1), compared to its isotropic form. The resulting TCS are much longer, consistent with observations (Artemyev, Angelopoulos, & Runov, 2016) and empirical reconstructions (M. I. Sitnov et al., 2019). We show this using 2D PIC simulations that are initialized by the TCS equilibria with quasi-adiabatic ions (M. I. Sitnov et al., 2003, hereafter the SGS model) whose description is simplified in the approximation of weak anisotropy (M. I. Sitnov & Arnold, 2022).

2 Weakly anisotropic TCS equilibrium with quasi-adiabatic ions

The SGS model had been originally proposed to explain Cluster observations of bifurcated ion-scale TCSs (Nakamura et al., 2002; Runov et al., 2003; Sergeev et al., 2003). It is based on the following generalization of the ion distribution function:

$$\begin{aligned} f_{0i} \propto \exp\left(\frac{q_i v_{Di}}{cT_{||i}}A_y - \frac{q_i\phi}{T_{||i}}\right)\exp\left\{-\frac{m_i[v_x^2+(v_y-v_{Di})^2+v_z^2]}{2T_{||i}}\right\} \\ \times\exp\left[\left(\frac{1}{T_{||i}}-\frac{1}{T_{\perp i}}\right)\frac{\Omega_i}{2}I_z^{(i)}\right] \end{aligned} \tag{3}$$

where $T_{||i}$ and $T_{\perp i}$ are the parallel and perpendicular ion temperature parameters, which become true temperatures outside the TCS where plasma is gyrotropic. The drift velocities $v_{D\alpha}$ determine the shift of electron and ion distributions in the y-direction and they determine the CS current in the Harris limit $T_{||i} = T_{\perp i}$; Ω_α is the particle gyrofrequency in the lobe field $B_0 = |B_x(|z| \to \infty)|$. The electron distribution was a shifted Maxwellian similar to the original Harris model.

Numerical solutions of Ampere's and Poisson's equations with the ion distribution (3) (M. I. Sitnov et al., 2003, 2006) showed that it indeed helps describe the effects of TCS bifurcation (when $T_{i||}/T_{i\perp} < 1$) and embedding (when $T_{i||}/T_{i\perp} > 1$). Moreover, the analysis of the corresponding 2-D solutions in the stretched field approximation ($B_z/B_0 \ll 1$) (M. I. Sitnov & Merkin, 2016) suggested that embedded TCS can be much longer, compared to their Harris analogs. However, it was unclear how the force balance could be changed in SGS, because use of the quasi-adiabatic invariant (3) yielded only diagonal components of the ion pressure tensor due to symmetry when $B_z = 0$. Being all different ($P_{ixx} \neq P_{iyy} \neq P_{izz}$), they provided agyrotropy but gave zero contribution to the third term in (1). At the same time, since numerical SGS solutions were computationally expensive, their verification in PIC simulations was limited to 1-D configurations with $B_z = 0$ (M. I. Sitnov et al., 2004, 2006).

An important advantage of SGS over other models with quasi-adiabatic ions (Kropotkin et al., 1997; M. I. Sitnov et al., 2000; L. M. Zelenyi et al., 2004) is the possibility of its reduction to the Harris model in the limit of isotropic ions. Moreover, in the most realistic case of weak ion anisotropy, one can expect a significant simplification of the model that would facilitate its PIC simulations. The corresponding weakly anisotropic approximation of SGS has been recently elaborated in (M. I. Sitnov & Arnold, 2022). It depends on two parameters, the ion anisotropy $\delta_1 = T_{i||}/T_{i\perp} - 1$ ($|\delta_1| \ll 1$) and the TCS embedding measure $\delta_2 = w_{Di}$, where $w_{D\alpha} = v_{D\alpha}/v_{T\perp\alpha}$ are the dimensionless drift velocities of the Harris component of the distribution (3) and its isotropic electron analog: δ_2 determines the ratio between the TCS thickness $L_{TCS} \sim \rho_{0i}$ and the Harris-like thick CS with the thickness $L_H = \rho_{0i}(v_{T\perp}/v_{Di})$ (Lembege & Pellat, 1982) in which the TCS is embedded.

In the double limit $|\delta_{1,2}| \ll 1$ and with the use of the dimensionless parameters $b = B_x/B_0$ and $\zeta = z/\rho_{\perp 0i}$, the TCS magnetic field can be presented in the form:

$$b(\zeta, \delta_1, \delta_2) = \sqrt{\tanh^2(\delta_2'\zeta_1(\zeta)) + \frac{4\delta_1 b^{(tcs)}(a^{(0)}(\zeta), \delta_2')}{\pi^2(1+\tau)\sqrt{2\delta_2}}} \Big/ \sqrt{1 + \frac{4\delta_1 b^{(tcs)}(\infty, \delta_2')}{\pi^2(1+\tau)\sqrt{2\delta_2}}}, \tag{4}$$

$$\frac{\zeta_1(\zeta)}{\zeta} \approx 1 + \frac{\delta_1(j_{(0)}^{(tcs)} - 2\delta_2' b^{(tcs)}(\infty, \delta_2'))}{(1+\tau)\pi^2\delta_2'\sqrt{2\delta_2}}\zeta^{(tcs)}(\zeta), \tag{5}$$

where $\delta_2' = \delta_2(1-\delta_1)$, $\tau = T_e/T_{\perp i}$; $j_{(0)}^{(tcs)}$ is a constant (≈ 1.77); $\zeta^{(tcs)}(\zeta)$ and $b^{(tcs)}(a, \delta)$ are universal functions determined in (M. I. Sitnov & Arnold, 2022).

In the isotropic limit $\delta_1 = 0$ this magnetic field formula is reduced to the conventional Harris solution $b = \tanh(\delta_2\zeta)$. Note that, to be able to be reduced to Harris, the original SGS solution was obtained with the additional constraint

$$w_{De} = -w_{Di}(1-\delta_1)\tau^{1/2}\mu^{1/2}, \tag{6}$$

where $\mu = m_e/m_i$ is electron-to-ion mass ratio. This constraint provides charge neutrality of the Harris solution and domination of the ion current as long as $\tau < 1$. It can be modified to describe negatively charged and electron dominated TCSs (Yoon & Lui, 2004; M. I. Sitnov et al., 2021).

The comparison of the approximation (4)-(5) with the exact numerical solution of the SGS model provided in Figure S1 of the Supporting Information (SI) reveals that it can be further improved if the Harris vector-potential there $a^{(0)}(\zeta)$ is replaced by its weakly anisotropic approximation (M. I. Sitnov & Arnold, 2022, Eq.(50)): $a(\zeta) = \log(\cosh(\zeta_1(\zeta)\delta_2'))/\delta_2'$.

The extension of this 1-D equilibrium to 2-D with a nonzero B_z magnetic field component can be provided following (Schindler, 1972) and (M. I. Sitnov & Merkin, 2016) to result in the formula

$$b(x,z) = \theta^{-1}(x) b^{(A)}(z\theta^{-1}(x), \delta_1, \delta_2), \tag{7}$$

where $\theta(x) = e^{\delta_2 a_1(x)}$, $a_1 = -A_y(x, z=0)/(B_0\rho_{\perp 0i})$ is the dimensionless vector-potential, and has the relation $d(\log(\theta))/dx = \varepsilon_1\delta_2/\rho_{\perp 0i}$ with the stretching parameter $\varepsilon_1 = B_z(x, z = 0)/B_0$. This 2D solution is not completely equivalent to the approximation $\delta_2 \to \delta_2\theta^{-1}(x)$ suggested in (M. I. Sitnov & Arnold, 2022). However, the difference is largely in the TCS correction terms $O(\delta_1)$ in (4). The corresponding profile of the magnetic field $B_z(x,z)$ is taken from the 2-D Harris-Schindler solution (M. I. Sitnov & Schindler, 2010, Eq.(4)), where we neglect the anisotropy dependence because B_z/B_0 is already a small parameter. The resulting 2-D solution is similar, but not equivalent, to Figure 12 in (M. I. Sitnov & Arnold, 2022). It is provided in Figure S2 where it is compared to the Harris solution with the same value of ε and comparable TCS thickness at $x = 0$. Note that since we neglected the anisotropy corrections in the B_z component, this solution does not obey the condition $\nabla \cdot \mathbf{B} = 0$. However, this inconsistency is fixed later in the PIC code, where the condition is provided at every time step using a multigrid algorithm (Press et al., 1996) and it results in only small corrections of the equilibrium picture.

3 PIC simulations

In order to test the new equilibrium laid out in (M. I. Sitnov & Arnold, 2022) we perform three 2D simulation runs that demonstrate that this quickly evolves to a true equilibrium with parameters applicable to Earth's magnetotail using the PIC code P3D (Zeiler et al., 2002). As is typical in PIC simulations, magnetic fields are normalized to the asymptotic value, B_0, lengths are normalized to the ion inertial length, d_i, times to the inverse ion cyclotron frequency, Ω_i^{-1}, masses to the ion mass, m_i, and densities to the maximum density in the simulation, n_0. Velocities are then normalized to the Alfvén speed, $C_A = B_0/\sqrt{4\pi n_0 m_i}$, and pressures to $P_0 = m_i n_0 C_A^2$. We also note that the distribution function is normalized to $f_0 = n_0/C_A^3$. Each run uses an ion to electron mass ratio, m_i/m_e, of 128, a speed of light equal to $15C_A$, an electron temperature of $0.1 m_i C_A^2$, and a nominal ion temperature of $0.4 m_i C_A^2$. Simulations are made in a box $80d_i \times 20d_i$ with a square grid cell of length $0.03d_i$ and a time step of $0.0025\Omega_i^{-1}$. The coordinates are chosen to be GSM-like with the x-axis directed opposite to the magnetic field line stretching (earthward) and z pointing up (northward). Simulations use the following values of the ion anisotropy and magnetic field stretching parameters: $\delta_1 = 0.2$ and $\varepsilon_1 = 0.03$ for Run 1; $\delta_1 = 0.1$ and $\varepsilon_1 = 0.03$ for Run 2; $\delta_1 = 0.2$ and $\varepsilon_1 = 0.1$ for Run 3. These values are consistent with estimates of δ_1 in the pre-onset (thinned) magnetotail current sheet (Yushkov et al., 2021) and other observations (Kaufmann et al., 2000; Artemyev et al., 2019) as well as the empirical picture of the tail stretching and thinning (M. I. Sitnov et al., 2019; Yushkov et al., 2021). More details on the simulation setup, including the boundary conditions employed, are provided in the SI.

In Figure 1 we show 2D distributions of the key parameters of the new equilibrium at the end of Run 1 ($\Omega_i t = 60$). The TCS embedding feature is clearly seen there from the comparison of Figures 1a and 1b: Unlike Harris-type CSs, the current density profile here is substantially narrower than that of the plasma density (the corresponding linear profiles are provided in Figure S3). Its key overstretching effect is seen in Figure 1b from the comparison of the current density isocontours (color boundaries) and the magnetic field lines: the former are stretched more than the latter. Figure S3 also reveals that the 2D SGS model is indeed selfconsistent and stable because the initial current and plasma density profiles given by the model don't change significantly by $\Omega_i t = 60$.

Figure 1c shows that that the local values of the temperature anisotropy $\delta_1^* = T_{i||}^*/T_{i\perp}^*$, where $T_{i||}^*$ and $T_{i\perp}^*$ are the local values of the parallel and perpendicular ion temperatures, are close to $\delta_1 = 0.2$ chosen as a global anisotropy parameter in the SGS model. But they may vary substantially, being reduced near the neutral plane $z = 0$ and at the boundaries, consistent with observations (Kaufmann et al., 2000, Figure 1).

Figure 1d shows that the plasma anisotropy is accompanied by a substantial agyrotropy measured here by the Q-parameter (Swisdak, 2016). Its value increases near the neutral plane where ions are less magnetized. It also increases tailward because of the reduction of the normal magnetic field near the right boundary (for details see the SI

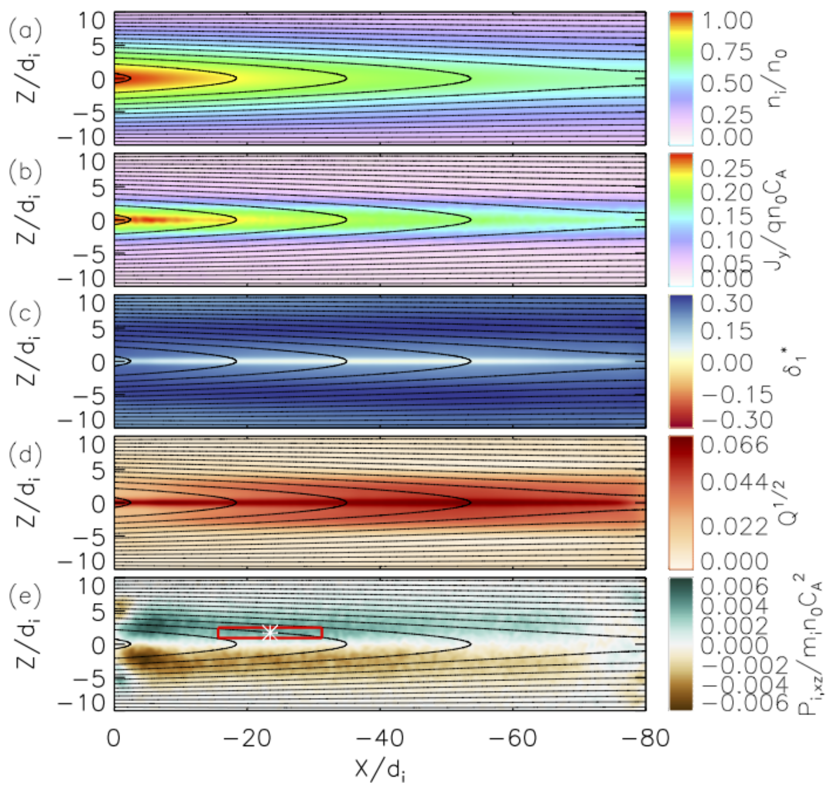

Figure 1. 2D distributions of the key parameters in Run 1 at the moment $t\Omega_i = 60$: (a-b) plasma and current densities; (c) ion anisotropy parameter δ_1^*; (d) ion agyrotropy parameter Q (Swisdak, 2016); (e) off-diagonal component of the ion pressure tensor $P_{i,xz}$ with magnetic field lines in black. The red box in (e) shows the location of the distribution function in Figure 3a and b, and the white star is the end point of the test particles in Figure 3f.

and refs. therein). Its peak value $Q^{1/2} \sim 0.1$ is consistent with observations (Motoba et al., 2022).

Perhaps the most intriguing feature of these simulations is provided by Figure 1e, which shows a small but substantial off-diagonal component, $P_{i,xz}$, of the pressure tensor. Moreover, being formally absent in the original SGS theory and resulting in the force imbalance at the beginning of the run (black dash-dotted line in Figure 2a), it is shown to increase during the run to eventually make a contribution to the force balance (1) comparable to the pressure gradient (cf. solid and dashed red lines in Figure 2b). To understand why it becomes possible in spite of weak plasma anisotropy, one can use the force balance outside the TCS analyzed by Rich et al. (1972). They noticed that the TCS reverses only a part of the antiparallel field component B_0 ($B_{TCS} \sim 0.5B_0$ in our simulations, according to Figure S3). As a result a small amount of anisotropy can balance 40% of the $\boldsymbol{J} \times \boldsymbol{B}$ force in Run 1. From Rich et al. (1972) the off diagonal component due to pressure anisotropy in the force balance equation is

$$(P_{||} - P_{\perp})B_xB_z/(B^2L_z) \approx 0.1/B^2\boldsymbol{J} \times \boldsymbol{B} \approx 0.4\boldsymbol{J} \times \boldsymbol{B} \tag{8}$$

Note that in real magnetotail TCSs this effect is even stronger because B_0/B_{TCS} ranges between 2.5 and 3.3 (Artemyev, Petrukovich, et al., 2011, Figure 4). As one can see from Figure 2c, the force balance is restored on the time scale $\Delta t \sim 10\Omega_i^{-1}$.

To reveal the energy range and hence the ion dynamic regime (adiabatic, chaotic or quasi-adiabatic) that provides the main contribution to the TCS overstretching effect, the distribution (3) was sampled in the red box from Figure 1e ($15.5d_i \times 1.5d_i$) and sliced into 30 energy annuli as is shown in Figure 3a. The comparison of its partial density distribution by the inner annulus radii (Figure 3c) and the contribution of the corresponding circles to the pressure tensor component $P_{i,xz}$ (Figure 3d) shows that this component is mainly provided by the suprathermal ions ($v > C_A$). Since for the parameters $\varepsilon_1 \ll 1$ and $L_z \sim \rho_{0i}$ used in our runs $\kappa \ll 1$ even for thermal ions, the overstretching effect and other non-Harris features must be provided by the quasi-adiabatic ions (Büchner & Zelenyi, 1989). Figure 3f shows test particle orbits that end at the white star location in Figure 1a. These test particles are chosen to have v_x, v_z corresponding to the green 'x' in Figure 3b. This location is at the peak in both the radius of the energy annuli, and θ, the location in the annulus associated with the largest contribution to $P_{i,xz}$ ($v_r \approx 1.3$ Figure 3d and $\theta \approx 0.6$ Figure 3e). They are then assigned a random v_y from a 1D maxwellian with temperature and drift speed equal to the local values ($\sim 0.4T_0$ and $\sim 0.13C_A$) and evolved backwards in time for $30\Omega_i^-1$ using the equilibrium magnetic field at $t\Omega_i = 60$ and no electric field. We plot 20 sample orbits that demonstrate that the figure-of-eight and meandering type orbits (cf. Speiser, 1965; Chen & Palmadesso, 1986; Büchner & Zelenyi, 1989) are responsible for generating the off diagonal pressure and hence the overstretching effect.

In Figure 4 we compare the current density profiles for Runs 1-3. This figure shows that the overstretching effect weakly depends on the anisotropy value (cf. Figures 4a and 4b), consistent with the theoretical estimates (M. I. Sitnov & Arnold, 2022). Figure 4c shows the effect of the reduction of the magnetic field stretching on the TCS structure. While the TCS becomes shorter, its current remains overstretched and stable. This stability is surprising because for $\varepsilon_1 = 0.1$ and the TCS thickness $L_{TCS} \approx 2\rho_{0i}$ the kappa parameter (Büchner & Zelenyi, 1989) approaches the upper limit of the quasi-adiabatic region. It was argued (Burkhart et al., 1992; Artemyev et al., 2019) that in this case the dominant ion population becomes chaotic and the equilibrium cannot be sustained. The reason of the TCS sustainability can be understood from Figure 3, which shows that the main contribution to the off-diagonal pressure tensor component $P_{i,xz}$ comes from the suprathermal ion population (cf. Figures 3a and 3b).

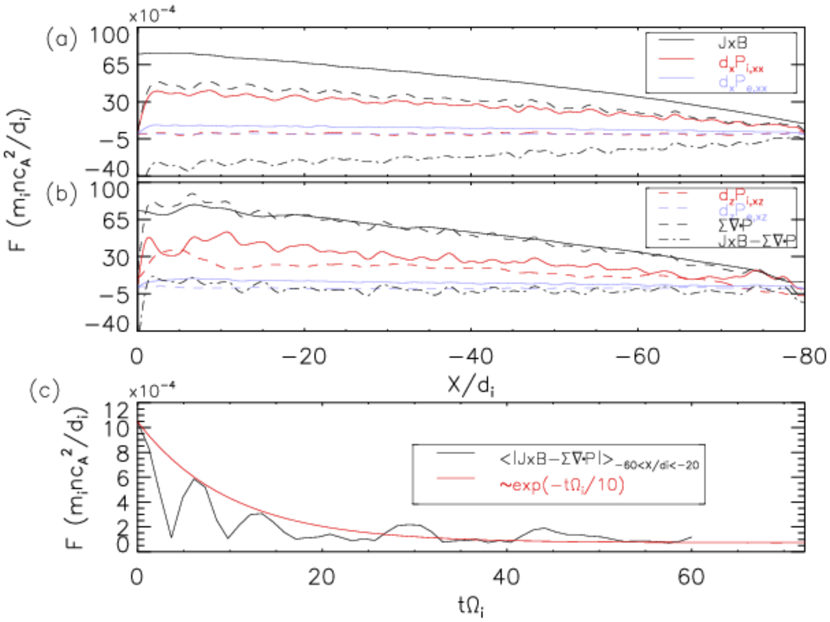

Figure 2. This shows the following quantities along the center of the current sheet at $t\Omega_i = 0$ (a) and 60 (b): $\boldsymbol{J} \times \boldsymbol{B}$ force in the x direction (black), the x-derivative of the diagonal ion (red) and electron (blue) pressure component, the z-derivative of the off diagonal ion (dashed red) and electron (dashed blue) pressure component, the sum of the divergence of the electron and ion pressure tensors in the x direction (dashed black), and the difference between the black and dashed black lines (dash-dot black). The latter should be near 0 for an equilibrium current sheet. (c) Shows the average value of the magnitude of the dash-dot black line between $x/d_i = -20$ and -60 as a function of time in black, and an exponential decay with time constant $10\Omega_i^{-1}$. Note that the current sheet reaches equilibrium by the end of the simulation. Similar figures for runs 2 and 3 can be found in Figures S4 and S5.

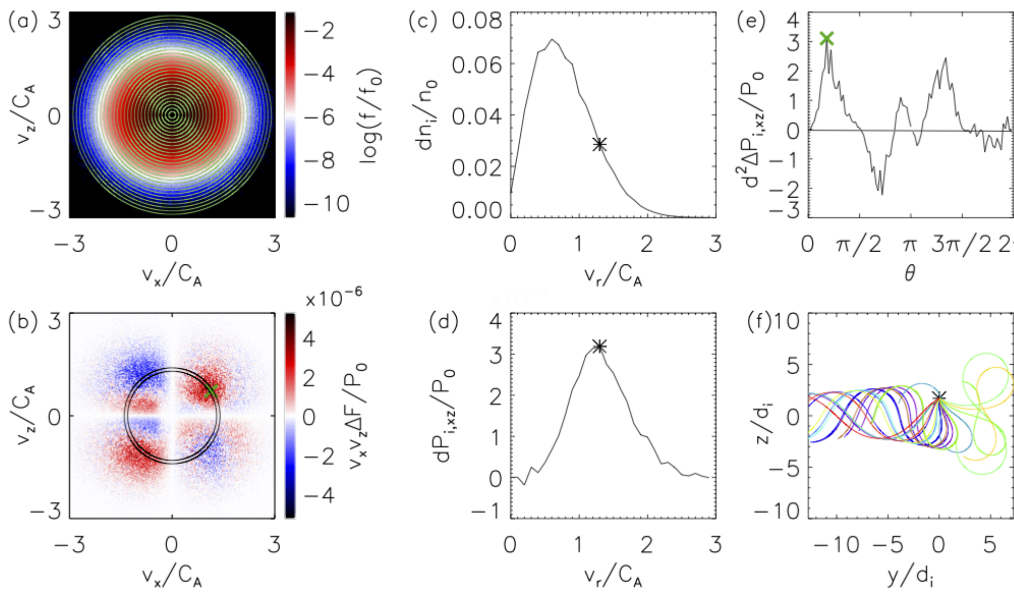

Figure 3. (a): the log of the distribution function taken from the red box in Figure 1a and integrated over v_y such that $n_i = \int f dv_x dv_z$. (b): the difference between the final and initial distributions, $\Delta F = m_i[f(t\Omega_i = 60) - f(t\Omega_i = 0)]dv_x dv_z$, multiplied by $v_x v_z$ to show phase space contributions to $P_{i,xz}$. (c) and (d): the contribution to the density and $P_{i,xz}$ respectively from each annulus bounded by the green circles centered at $(0,0)$ in (a) with radii, v_r, uniformly spaced at $0.1C_A$, where $dP_{i,xz} = m_i \int_0^{2\pi} v_x v_z f v_r d\theta dv_r$ and similarly for dn_i. (e): the contribution from the annulus $1.3 < v_r/C_A < 1.4$ shown in (b), and marked by the star in (c) and (d), to $P_{i,xz}$ as a function of the polar angle θ, where $d^2\Delta P_{i,xz} = m_i v_x v_z[f(t\Omega_i = 60) - f(t\Omega_i = 0)]v_r dv_r d\theta$. (f): sample test particle orbits with final velocities located at the green 'x' in (b) and correspond to the green 'x' in (e), and final positions located at the star in (f) and Figure 1(e).

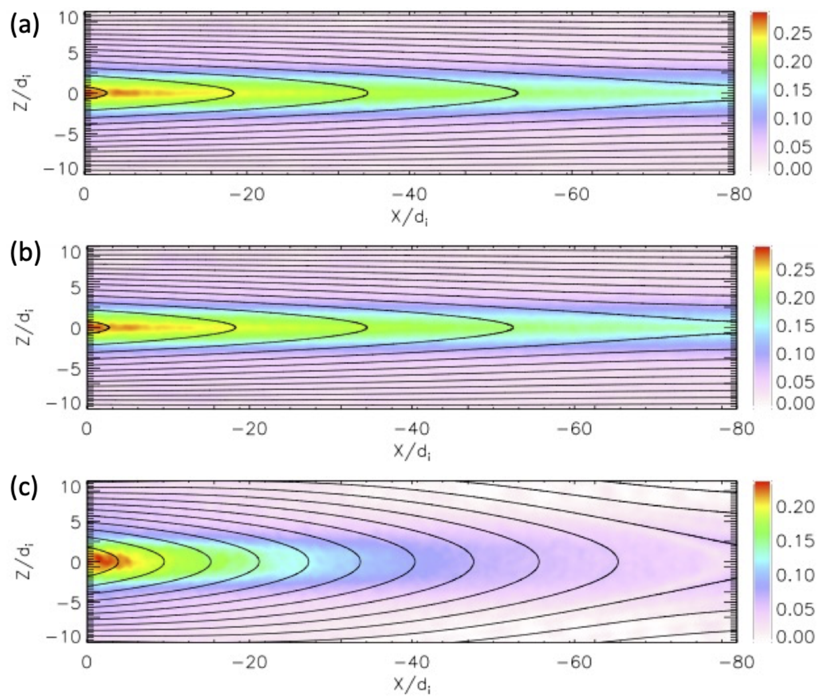

Figure 4. 2D distributions of the total current density J_y/qn_0C_A at $t\Omega_i = 30$ for (a) Run 1 with $\delta_1 = 0.2$ and $\varepsilon_1 = 0.03$, (b) Run 2 with $\delta_1 = 0.1$ and $\varepsilon_1 = 0.03$, and (c) Run 3 with $\delta_1 = 0.2$ and $\varepsilon_1 = 0.1$.

4 Discussion and Conclusion

In this paper we described for the first time in PIC simulations the selfconsistent structure and evolution of a new class of thin ion-scale TCSs whose current distributions are substantially overstretched compared to the magnetic field lines (Figures 1 and 4) so that their aspect ratio L_x/L_z exceeds their magnetic field line stretching B_0/B_z unlike isotropic Harris-type models. Such a violation of the isotropic force balance can be provided by the relatively small values of the ion anisotropy outside the TCS if the latter reverses only a part (B_{TCS}) of the antiparallel field component B_0 because then it increases the off-diagonal component of the ion pressure $P_{xz} = (P_{||} - P_{\perp})B_xB_z/B^2$.

It is found (Figure 3) that the non-isotropic force balance is provided by quasi-adiabatic (Speiser) ion orbits. While the corresponding ion distribution (3) based on the quasi-adiabatic invariant (2) is already agyrotropic, its off-diagonal components are zero and it cannot maintain the force balance necessary for the corresponding 2D equilibrium solution (M. I. Sitnov & Arnold, 2022). However, Figure 2 shows that the necessary force balance is restored rather quickly and likely due to bending of the corresponding Speiser orbits in the actual (stretched rather than antiparallel) magnetic field. According to Figures 3c-3d, the main contribution to the force balance modification is made by suprathermal ions closer to the tail of their distribution. This explains the absence of any CS catastrophe reported in earlier single-particle models (Burkhart et al., 1992) with the increase of the normal magnetic field (Figure 4c).

Note that, unlike Harris CS, the new SGS equilibria help explain such important observational features of the magnetotail CS as their cooling and density increase during the thinning process (Runov et al., 2021; Yushkov et al., 2021). This is because the SGS current thickness scales as the ion gyroradius $\rho_{0i} \propto T_i^{1/2}$ (M. I. Sitnov et al., 2003), which is also close to the ion inertial length $d_i \propto n_i^{-1/2}$ when the plasma anisotropy is small (M. I. Sitnov & Arnold, 2022). Note also that the embedded structure of the obtained selfconsistent CS is consistent with observations (Runov et al., 2005; Runov et al., 2006) and global hybrid simulations (Lu et al., 2016).

Simulations show that after establishing the new force balance, the TCS equilibria remain stable, contrary to theoretical suggestions of their destabilization, albeit for strong anisotropy regimes (L. Zelenyi et al., 2008). It is yet unknown if this stability is due to the electron compressibility effect suggested by Lembege and Pellat (1982) for 2D Harris models and if it can be relaxed for local magnetic flux accumulation regions with the tailward B_z gradient, as suggested by M. I. Sitnov and Schindler (2010). Further simulations are also necessary to clarify the role of the TCS negative charging (Lu et al., 2020; M. Sitnov et al., 2021), electron current domination (Lu et al., 2020; M. I. Sitnov et al., 2021) and the effect of external driving (Hesse & Schindler, 2001; Liu et al., 2014; M. Sitnov et al., 2021; M. I. Sitnov et al., 2021). But the present study solves a fundamental problem of the ion-scale TCS formation sufficiently far from Earth where TCSs necessary for reconnection and the resulting X-lines are indeed observed.

5 Open Research

The data used in this paper are archived on Zenodo along with the necessary files to reproduce the figures using IDL (https://doi.org/10.5281/zenodo.7927177).

Acknowledgments
The authors thank Anton Artemyev, Ari Le, and Adam Michael for useful discussions. The work on this paper benefited from the discussions at the ISSI workshop"Magnetotail Dipolarizations: Archimedes Force or Ideal Collapse?" held in Bern, Switzerland, 16-20 May 2022. This study also benefited greatly from interesting discussions within the framework of the NASA LWS Team "Fast Reconnection Onset". This work was funded by NASA grants 80NSSC20K1271 and 80NSSC20K1787, as well as the NSF grant AGS-1744269. Simulations were made possible by the NCAR's computational and information systems laboratory (http://doi.org/10.5065/D6RX99HX), supported by the NSF, as well as the NASA high-end computing program through the NASA advanced supercomputing division at Ames Research Center.

References

Angelopoulos, V., Artemyev, A., Phan, T. D., & Miyashita, Y. (2020, Mar 01). Near-earth magnetotail reconnection powers space storms. *Nature Physics*, *16*(3), 317-321. Retrieved from `https://doi.org/10.1038/s41567-019-0749-4` doi: 10.1038/s41567-019-0749-4

Artemyev, A. V., Angelopoulos, V., & Runov, A. (2016). On the radial force balance in the quiet time magnetotail current sheet. *Journal of Geophysical Research: Space Physics*, *121*(5), 4017-4026. doi: https://doi.org/10.1002/2016JA022480

Artemyev, A. V., Angelopoulos, V., Vasko, I. Y., Zhang, X.-J., Runov, A., & Zelenyi, L. M. (2019). Ion anisotropy in earth's magnetotail current sheet: Multicomponent ion population. *Journal of Geophysical Research: Space Physics*, *124*(5), 3454-3467. doi: 10.1029/2019JA026604

Artemyev, A. V., Baumjohann, W., Petrukovich, A. A., Nakamura, R., Dandouras, I., & Fazakerley, A. (2011). Proton/electron temperature ratio in the magnetotail. *Annales Geophysicae*, *29*(12), 2253–2257. Retrieved from `https://angeo.copernicus.org/articles/29/2253/2011/` doi: 10.5194/angeo-29-2253-2011

Artemyev, A. V., Petrukovich, A. A., Nakamura, R., & Zelenyi, L. M. (2011). Cluster statistics of thin current sheets in the earth magnetotail: Specifics of the dawn flank, proton temperature profiles and electrostatic effects. *Journal of Geophysical Research: Space Physics*, *116*(A9). doi: https://doi.org/10.1029/2011JA016801

Artemyev, A. V., Petrukovich, A. A., Nakamura, R., & Zelenyi, L. M. (2012). Adiabatic electron heating in the magnetotail current sheet: Cluster observations and analytical models. *Journal of Geophysical Research: Space Physics*, *117*(A6). doi: https://doi.org/10.1029/2012JA017513

Artemyev, A. V., Petrukovich, A. A., Nakamura, R., & Zelenyi, L. M. (2015). Two-dimensional configuration of the magnetotail current sheet: Themis observations. *Geophysical Research Letters*, *42*(10), 3662-3667. doi: https://doi.org/10.1002/2015GL063994

Artemyev, A. V., Vasko, I. Y., Angelopoulos, V., & Runov, A. (2016). Effects of electron pressure anisotropy on current sheet configuration. *Physics of Plasmas*, *23*(9), 092901. Retrieved from `https://doi.org/10.1063/1.4961926` doi: 10.1063/1.4961926

Bessho, N., & Bhattacharjee, A. (2014). Instability of the current sheet in the Earth's magnetotail with normal magnetic field. *Phys. Plasmas*, *21*(1), 102905.

Birn, J., Schindler, K., & Hesse, M. (2004). Thin electron current sheets and their relation to auroral potentials. *Journal of Geophysical Research: Space Physics*, *109*(A2). doi: https://doi.org/10.1029/2003JA010303

Büchner, J., & Zelenyi, L. M. (1989). Regular and chaotic charged particle motion in magnetotaillike field reversals: 1. basic theory of trapped motion. *Journal of Geophysical Research: Space Physics*, *94*(A9), 11821-11842. doi: https://doi.org/10.1029/JA094iA09p11821

Burkhart, G. R., Drake, J. F., Dusenbery, P. B., & Speiser, T. W. (1992). A particle model for magnetotail neutral sheet equilibria. *Journal of Geophysical Research: Space Physics*, *97*(A9), 13799-13815. doi: https://doi.org/10.1029/92JA00495

Chen, J., & Palmadesso, P. J. (1986). Chaos and nonlinear dynamics of single-particle orbits in a magnetotaillike magnetic field. *Journal of Geophysical Research: Space Physics*, *91*(A2), 1499-1508. doi: https://doi.org/10.1029/JA091iA02p01499

Coppi, B., Laval, G., & Pellat, R. (1966). Dynamics of the geomagnetic tail. *Physical Review Letters*, *16*(2), 1207–1210. doi: 10.1103/PhysRevLett.16.1207

Eastwood, J. P., Phan, T. D., Øieroset, M., & Shay, M. A. (2010). Average properties of the magnetic reconnection ion diffusion region in the earth's magnetotail: The 2001-2005 cluster observations and comparison with simulations. *Journal of Geophysical Research: Space Physics*, *115*(A8). doi: https://doi.org/10.1029/2009JA014962

Egedal, J., Le, A., & Daughton, W. (2013). A review of pressure anisotropy caused by electron trapping in collisionless plasma, and its implications for magnetic reconnection. *Physics of Plasmas*, *20*(6), 061201. Retrieved from `https://doi.org/10.1063/1.4811092` doi: 10.1063/1.4811092

Harris, E. (1962). On a plasma sheath separating regions of oppositely directed magnetic field. *Il Nuovo Cimento Series 10*, *23*(1), 115-121. Retrieved from `http://dx.doi.org/10.1007/BF02733547` doi: 10.1007/BF02733547

Hesse, M., & Schindler, K. (2001). The onset of magnetic reconnection in the magnetotail. *Earth, Planets and Space*, *53*, 645–653.

Kaufmann, R. L., Ball, B. M., Paterson, W. R., & Frank, L. A. (2000). Pressure anisotropy and by in the magnetotail current sheet. In *Magnetospheric current systems* (p. 323-330). American Geophysical Union (AGU). Retrieved from `https://agupubs.onlinelibrary.wiley.com/doi/abs/10.1029/GM118p0323` doi: https://doi.org/10.1029/GM118p0323

Kropotkin, A. P., Malova, H. V., & Sitnov, M. I. (1997). Self-consistent structure of a thin anisotropic current sheet. *Journal of Geophysical Research: Space Physics*, *102*(A10), 22099-22106. doi: https://doi.org/10.1029/97JA01316

Le, A., Stanier, A., Daughton, W., Ng, J., Egedal, J., Nystrom, W. D., & Bird, R. (2019). Three-dimensional stability of current sheets supported by electron pressure anisotropy. *Physics of Plasmas*, *26*(10), 102114. Retrieved from `https://doi.org/10.1063/1.5125014` doi: 10.1063/1.5125014

Lembege, B., & Pellat, R. (1982). Stability of a thick two-dimensional quasineutral sheet. *Phys. Fluids*, *25*, 1995–2004. doi: 10.1063/1.863677

Liu, Y.-H., Birn, J., Daughton, W., Hesse, M., & Schindler, K. (2014). Onset of reconnection in the near magnetotail: PIC simulations. *Journal of Geophysical Research: Space Physics*, *119*(12), 9773–9789. Retrieved from `http://dx.doi.org/10.1002/2014JA020492` doi: 10.1002/2014JA020492

Lu, S., Angelopoulos, V., Artemyev, A. V., Jia, Y., Chen, Q., Liu, J., & Runov, A. (2020). Magnetic reconnection in a charged, electron-dominant current sheet. *Physics of Plasmas*, *27*(10), 102902. doi: 10.1063/5.0020857

Lu, S., Lin, Y., Angelopoulos, V., Artemyev, A. V., Pritchett, P. L., Lu, Q., & Wang, X. Y. (2016). Hall effect control of magnetotail dawn-dusk asymmetry: A three-dimensional global hybrid simulation. *Journal of Geophysical Research: Space Physics*, *121*(12), 11,882-11,895. doi: 10.1002/2016JA023325

McPherron, R. L. (2016). Where and when does reconnection occur in the tail? *Journal of Geophysical Research: Space Physics*, *121*(5), 4607-4610. doi: https://doi.org/10.1002/2015JA022258

Merkin, V. G., Panov, E. V., Sorathia, K. A., & Ukhorskiy, A. Y. (2019). Contribution of bursty bulk flows to the global dipolarization of the magnetotail during an isolated substorm. *Journal of Geophysical Research: Space Physics*, *124*(11), 8647-8668. doi: https://doi.org/10.1029/2019JA026872

Motoba, T., Sitnov, M. I., Stephens, G. K., & Gershman, D. J. (2022). A new perspective on magnetotail electron and ion divergent flows: Mms observations. *Journal of Geophysical Research: Space Physics*, *127*(10), e2022JA030514. doi: https://doi.org/10.1029/2022JA030514

Nagai, T., Fujimoto, M., Nakamura, R., Baumjohann, W., Ieda, A., Shinohara, I., ... Mukai, T. (2005). Solar wind control of the radial distance of the magnetic reconnection site in the magnetotail. *Journal of Geophysical Research: Space Physics*, *110*(A9). doi: https://doi.org/10.1029/2005JA011207

Nagai, T., Shinohara, I., & Zenitani, S. (2015). The dawn-dusk length of the x line in the near-earth magnetotail: Geotail survey in 1994-2014. *Journal of Geophysical Research: Space Physics*, *120*(10), 8762-8773. doi: 10.1002/2015JA021606

Nakamura, R., Baumjohann, W., Runov, A., Volwerk, M., Zhang, T. L., Klecker, B., ... Frey, H. U. (2002). Fast flow during current sheet thinning. *Geophysical Research Letters*, *29*(23), 55-1-55-4. doi: 10.1029/2002GL016200

Press, W. H., Teukolsky, S. a., Vetterling, W. T., & Flannery, B. P. (1996). *Numerical Recipes in Fortran 77: the Art of Scientific Computing. Second Edition* (Vol. 1).

Pritchett, P. L. (2015). Instability of current sheets with a localized accumulation of magnetic flux. *Physics of Plasmas*, *22*(6), -. Retrieved from `http://scitation.aip.org/content/aip/journal/pop/22/6/10.1063/1.4921666` doi: http://dx.doi.org/10.1063/1.4921666

Pritchett, P. L., Coroniti, F. V., Pellat, R., & Karimabadi, H. (1991). Collisionless reconnection in two-dimensional magnetotail equilibria. *Journal of Geophysical Research: Space Physics*, *96*(A7), 11523-11538. doi: https://doi.org/10.1029/91JA01094

Rich, F. J., Vasyliunas, V. M., & Wolf, R. A. (1972). On the balance of stresses in the plasma sheet. *Journal of Geophysical Research (1896-1977)*, *77*(25), 4670-4676. doi: 10.1029/JA077i025p04670

Runov, A., Angelopoulos, V., Artemyev, A., Weygand, J., Lu, S., Lin, Y., & Zhang, X.-J. (2021). Global and local processes of thin current sheet formation during substorm growth phase. *Journal of Atmospheric and Solar-Terrestrial Physics*, *220*, 105671. Retrieved from `https://www.sciencedirect.com/science/article/pii/S1364682621001280` doi: https://doi.org/10.1016/j.jastp.2021.105671

Runov, A., Nakamura, R., Baumjohann, W., Zhang, T. L., Volwerk, M., Eichelberger, H.-U., & Balogh, A. (2003). Cluster observation of a bifurcated current sheet. *Geophysical Research Letters*, *30*(2). doi: https://doi.org/10.1029/2002GL016136

Runov, A., Sergeev, V. A., Baumjohann, W., Nakamura, R., Apatenkov, S., Asano, Y., … Rème, H. (2005). Electric current and magnetic field geometry in flapping magnetotail current sheets. *Annales Geophysicae*, *23*(4), 1391–1403. Retrieved from `https://angeo.copernicus.org/articles/23/1391/2005/` doi: 10.5194/angeo-23-1391-2005

Runov, A., Sergeev, V. A., Nakamura, R., Baumjohann, W., Apatenkov, S., Asano, Y., … Balogh, A. (2006). Local structure of the magnetotail current sheet: 2001 Cluster observations. *Annales Geophysicae*, *24*(1), 247-262. doi: 10.5194/angeo-24-247-2006

Schindler, K. (1965). Adiabatic particle orbits in discontinuous fields. *Journal of Mathematical Physics*, *6*(2), 313-321. doi: 10.1063/1.1704282

Schindler, K. (1972). A selfconsistent theory of the tail of the magnetosphere. In *Earth's Magnetospheric Processes, B.M. McCormac, ed.* (pp. 200–209). Dordrecht-Holland: D. Reidel.

Schindler, K. (1974). A theory of the substorm mechanism. *J. Geophys. Res.*, *79*(19), 2803–2810. doi: 10.1029/JA079i019p02803

Schindler, K., & Birn, J. (2002). Models of two-dimensional embedded thin current sheets from vlasov theory. *Journal of Geophysical Research: Space Physics*, *107*(A8), SMP 20-1-SMP 20-13. doi: https://doi.org/10.1029/2001JA000304

Sergeev, V., Runov, A., Baumjohann, W., Nakamura, R., Zhang, T. L., Volwerk, M., … Klecker, B. (2003). Current sheet flapping motion and structure observed by cluster. *Geophysical Research Letters*, *30*(6). doi: https://doi.org/10.1029/2002GL016500

Sitnov, M., Birn, J., Ferdousi, B., Gordeev, E., Khotyaintsev, Y., Merkin, V., … Zhou, X. (2019, 16). Explosive magnetotail activity. *Space Science Reviews*, *215*(4), 31. Retrieved from `https://doi.org/10.1007/s11214-019-0599-5` doi: 10.1007/s11214-019-0599-5

Sitnov, M., Stephens, G., Motoba, T., & Swisdak, M. (2021). Data mining reconstruction of magnetotail reconnection and implications for its first-principle modeling. *Frontiers in Physics*, *0*(0). doi: 10.3389/fphy.2021.644884

Sitnov, M. I., & Arnold, H. (2022). Equilibrium kinetic theory of weakly anisotropic embedded thin current sheets. *Journal of Geophysical Research: Space Physics*, *127*(11), e2022JA030945. doi: https://doi.org/10.1029/2022JA030945

Sitnov, M. I., Buzulukova, N., Swisdak, M., Merkin, V. G., & Moore, T. E. (2013). Spontaneous formation of dipolarization fronts and reconnection onset in the magnetotail. *Geophys. Res. Lett.*, *40*(1), 22–27. doi: 10.1029/2012GL054701

Sitnov, M. I., Guzdar, P. N., & Swisdak, M. (2003). A model of the bifurcated current sheet. *Geophysical Research Letters*, *30*(13). doi: https://doi.org/10.1029/2003GL017218

Sitnov, M. I., & Merkin, V. G. (2016). Generalized magnetotail equilibria: Effects of the dipole field, thin current sheets, and magnetic flux accumulation. *Journal of Geophysical Research: Space Physics*, *121*(8), 7664–7683. Retrieved from `http://dx.doi.org/10.1002/2016JA023001` doi: 10.1002/2016JA023001

Sitnov, M. I., Merkin, V. G., Roytershteyn, V., & Swisdak, M. (2018). Kinetic dissipation around a dipolarization front. *Geophysical Research Letters*, *45*(10), 4639-4647. Retrieved from `https://agupubs.onlinelibrary.wiley.com/doi/abs/10.1029/2018GL077874` doi: 10.1029/2018GL077874

Sitnov, M. I., Motoba, T., & Swisdak, M. (2021). Multiscale nature of the magnetotail reconnection onset. *Geophysical Research Letters*, *48*(10), e2021GL093065. doi: https://doi.org/10.1029/2021GL093065

Sitnov, M. I., & Schindler, K. (2010). Tearing stability of a multiscale magnetotail current sheet. *Geophys. Res. Lett.*, *37*, 08102. doi: 10.1029/2010GL042961

Sitnov, M. I., Stephens, G. K., Tsyganenko, N. A., Miyashita, Y., Merkin, V. G., Motoba, T., ... Genestreti, K. J. (2019). Signatures of nonideal plasma evolution during substorms obtained by mining multimission magnetometer data. *Journal of Geophysical Research: Space Physics*, *124*(11), 8427-8456. doi: 10.1029/2019JA027037

Sitnov, M. I., & Swisdak, M. (2011). Onset of collisionless magnetic reconnection in two-dimensional current sheets and formation of dipolarization fronts. *J. Geophys. Res.*, *116*(A), 12216. doi: 10.1029/2011JA016920

Sitnov, M. I., Swisdak, M., Drake, J. F., Guzdar, P. N., & Rogers, B. N. (2004). A model of the bifurcated current sheet: 2. flapping motions. *Geophysical Research Letters*, *31*(9). doi: https://doi.org/10.1029/2004GL019473

Sitnov, M. I., Swisdak, M., Guzdar, P. N., & Runov, A. (2006). Structure and dynamics of a new class of thin current sheets. *Journal of Geophysical Research: Space Physics*, *111*(A8). doi: https://doi.org/10.1029/2005JA011517

Sitnov, M. I., Zelenyi, L. M., Malova, H. V., & Sharma, A. S. (2000). Thin current sheet embedded within a thicker plasma sheet: Self-consistent kinetic theory. *Journal of Geophysical Research: Space Physics*, *105*(A6), 13029-13043. doi: https://doi.org/10.1029/1999JA000431

Sonnerup, B. U. O. (1971). Adiabatic particle orbits in a magnetic null sheet. *Journal of Geophysical Research (1896-1977)*, *76*(34), 8211-8222. doi: https://doi.org/10.1029/JA076i034p08211

Speiser, T. W. (1965). Particle trajectories in model current sheets: 1. analytical solutions. *Journal of Geophysical Research (1896-1977)*, *70*(17), 4219-4226. doi: https://doi.org/10.1029/JZ070i017p04219

Stephens, G. K., Sitnov, M. I., Weigel, R. S., Turner, D. L., Tsyganenko, N. A., Rogers, A. J., ... Slavin, J. A. (2023). Global structure of magnetotail reconnection revealed by mining space magnetometer data. *Journal of Geophysical Research: Space Physics*, *128*(2), e2022JA031066. doi: https://doi.org/10.1029/2022JA031066

Swisdak, M. (2016). Quantifying gyrotropy in magnetic reconnection. *Geophysical Research Letters*, *43*(1), 43-49. doi: 10.1002/2015GL066980

Wang, C.-P., Gkioulidou, M., Lyons, L. R., & Angelopoulos, V. (2012). Spatial distributions of the ion to electron temperature ratio in the magnetosheath and plasma sheet. *Journal of Geophysical Research: Space Physics*, *117*(A8). doi: https://doi.org/10.1029/2012JA017658

Yoon, P. H., & Lui, A. T. Y. (2004). Model of ion- or electron-dominated current sheet. *Journal of Geophysical Research: Space Physics*, *109*(A11). doi: 10.1029/2004JA010555

Yushkov, E. V., Petrukovich, A. A., Artemyev, A. V., & Nakamura, R. (2021). Thermodynamics of the magnetotail current sheet thinning. *Journal of Geophysical Research: Space Physics*, *126*(4), e2020JA028969. doi: https://doi.org/10.1029/2020JA028969

Zeiler, A., Biskamp, D., Drake, J. F., Rogers, B. N., Shay, M. A., & Scholer, M. (2002). Three-dimensional particle simulations of collisionless magnetic reconnection. *J. Geophys. Res.*, *107*(A), 1230. doi: 10.1029/2001JA000287

Zelenyi, L., Artemiev, A., Malova, H., & Popov, V. (2008). Marginal stability of thin current sheets in the Earth's magnetotail. *J. Atm. Sol.-Terr. Phys.*, *70*(2–4), 325–333. doi: 10.1016/j.jastp.2007.08.019

Zelenyi, L. M., Malova, H. V., Popov, V. Y., Delcourt, D., & Sharma, A. S. (2004). Nonlinear equilibrium structure of thin currents sheets: influence of electron pressure anisotropy. *Nonlinear Processes in Geophysics*, *11*(5/6), 579–587. Retrieved from https://npg.copernicus.org/articles/11/579/2004/ doi: 10.5194/npg-11-579-2004